analytical chemistry

Article

pubs.acs.org/ac

Electrochemiluminescent Quenching of Quantum Dots for Ultrasensitive Immunoassay through Oxygen Reduction Catalyzed by Nitrogen-Doped Graphene-Supported Hemin

Shengyuan Deng, Jianping Lei, Yin Huang, Yan Cheng, and Huangxian Ju*

State Key Laboratory of Analytical Chemistry for Life Science, Department of Chemistry, Nanjing University, Nanjing 210093, China

ABSTRACT: A hemin functionalized graphene sheet was prepared via the noncovalent assembly of hemin on nitrogen-doped graphene. The graphene sheet could act as an oxygen reduction catalyst to produce sensitive electrochemiluminescent (ECL) quenching of quantum dots (QDs) due to the annihilation of dissolved oxygen, the ECL coreactant, by its electrocatalytic reduction. With the use of the catalyst with high loading of hemin as a signal tag of the secondary antibody, a novel ultrasensitive immunoassay method for biomarker detection was proposed. In an air-saturated pH 8.0 buffer, the immunosensor constructed by a stepwise immobilization of bidentate-chelated CdTe QDs and capture antibody showed an intensive cathodic ECL irradiation, which could be scavenged upon the formation of the catalyst-bound sandwich immunocomplex. With the use of the carcinoembryonic antigen as a model analyte, the immunoassay method showed a linear range from 0.1 pg mL^{-1} to 10 ng mL^{-1} and a detection limit of 24 fg mL^{-1}. The immunosensor exhibited good stability, acceptable fabrication reproducibility, and practicability. The electrocatalytic reduction-based ECL quenching strategy provided a powerful avenue for the design of the ultrasensitive detection method, showing great promise for clinical application.

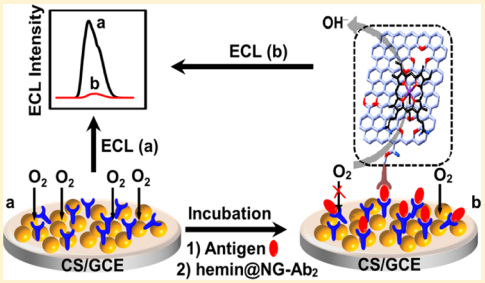

Highly sensitive and selective determination of protein biomarkers is essential to many areas, including disease diagnosis, biomedical research, and biodefense applications.[1−3]

Great efforts, involving electrochemical, fluorescent, chemiluminescent, and electrochemiluminescent (ECL) techniques, have been endeavored to develop ultrasensitive immunosensors especially for the detection of low-abundance biomarkers.[4−6] Owing to the intrinsic low background and high sensitivity of quantum dots (QDs)-based ECL analytical technique, several signal amplification strategies based on nanomaterials and/or enzymes have been designed for developing ultrasensitive ECL immunoassays.[4,7] The consumption of a coreactant is one primary ECL methodology through enzymatic reactions on the immunosensor surface. Typically, H_2O_2 as a conventional coreactant produced in the cathodic reduction of dissolved oxygen can be consumed by oxidizing hydroquinone in the presence of horseradish peroxidase (HRP)-labeled antibody,[8] resulting in a target concentration-dependent decrease of the ECL emission. However, the catalytic activity of natural enzyme strictly counts on its conformation and specific substrate,[9] and the relatively large occupied volume also restrains its loading capacity on miscellaneous nanocarriers.[10,11] Hence, searching for an enzymelike mimic with high-loading capacity for labeling signal antibody is of great importance for the immunoassay.

Since HRP is structurally an iron-containing porphyrin complex, mimicking the bioactivity of HRP with iron porphyrin such as hemin has recently brought about considerable concern.[12,13] However, the direct application of hemin as a biomimetic catalyst is very difficult since its molecular aggregation in aqueous solution causes catalytically inactive dimers and oxidative self-destruction in the oxidizing media.[14] Thus, it has often been assembled in a composite as enzyme-mimicking analogue to perform the catalytic reaction. An extensively concerned example is the assembly of *G*-quadruplex-based DNAzyme by the conjugation of hemin to single-stranded guanine-rich nucleic acid,[15] which has been considered as a successful artificial apo-enzyme to simulate the activity of HRP.[16] Another avenue is to assemble the hemin on nanostructures such as graphene oxide (GO)[17] through covalent and noncovalent interactions. However, in consideration of the fact that in natural enzymes, the heme group is actually axially coordinated with a proximal histidine-terminated peptide residue,[18] the assembly via axial ligation is favorable for restoring the primitive chemical environment of the mimetic enzyme. Although hemin has been normally used as an HRP mimic, its capability as oxygen reduction catalyst has rarely been reported. Here, a novel oxygen reduction catalyst was designed by the noncovalent assembly of hemin on nitrogen-doped graphene (NG). The hemin@NG showed sensitive ECL quenching of QDs due to the annihilation of dissolved oxygen, the ECL coreactant, by its electrocatalytic reduction. Thus, a new ultrasensitive immunoassay method was further proposed by using the electrocatalyst as a signal tag.

Compared with GO, the doping of nitrogen into carbon backbones offers a greater convenience for immobilization of iron porphyrin due to the axial coordination between the iron

Received: December 17, 2012
Accepted: May 9, 2013
Published: May 9, 2013

   dx.doi.org/10.1021/ac3036537 | *Anal. Chem.* 2013, 85, 5390−5396

active center and the pyridinic N originated from defective sites.[19,20] Moreover, N atoms as the active sites in NG can act as electron donors to promote the reactivity of adsorbed molecules, especially to facilitate the electrocatalytic reduction of O_2.[21,22] Thus hemin@NG can theoretically produce higher catalytic efficiency than hemin@GO to quench the cathodic ECL emission of QDs. With a sandwich immunoassay format using an immunosensor constructed by immobilization of bidentate-chelated CdTe QDs and capture antibody (Scheme 1), the hemin@NG as a tracing tag showed higher sensitivity.

Scheme 1. Schematic Illustration of Hemin@Ng as Signal Tag for QD-Based ECL Immunoassay

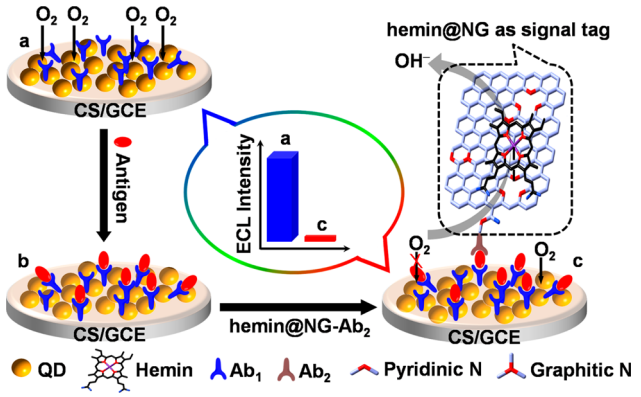

With the use of a carcinoembryonic antigen (CEA) as a model, the proposed ultrasensitive immunoassay method could detect the protein biomarker down to the subpicomolar level with a detection range over 5 orders of magnitude. The utilization of the NG nanosheet as the signal tag in QD-based ECL systems could avoid the "blackbody effect".[23] The hemin@N-doped carbon nanomaterials provided not only a facile avenue for the direct assembly of hemin on nanostructures but also a novel substitute of natural enzyme for signal amplification of the ECL immunoassay. This avenue could easily be extended to other porphyrin derivatives for their applications in bioassay.

EXPERIMENTAL SECTION

Materials and Reagents. Horseradish peroxidase (HRP), chitosan (from crab shell, purity ≥85%, deacetylation), *N*-hydroxysulfosuccinimide (NHS), 1-ethyl-3-(3-dimethylaminopropyl) carbodiimide (EDC), *N*-2-(4-morpholino)-ethanesulfonic acid (MES), and bovine serum albumin (BSA) were purchased from Sigma-Aldrich Chemical Company, Ltd. (Shanghai, China). Cadmium chloride ($CdCl_2 \cdot 2.5H_2O$), *meso*-2,3-dimercaptosuccinic acid (DMSA), and glutaraldehyde (25% aqueous solution) were purchased from Alfa Aesar Company, Ltd. (Tianjin, China). Nitrogen-doped graphene (NG, purity >99%) with the N content of 5.21% was bought from Nanjing Hope Analytical Equipment Company Ltd. (Nanjing, China). Carboxylic graphene oxide (GO, purity >99.8%) was purchased from Nanjing XFNano Materials Tech Company Ltd. (Nanjing, China). Carcinoembryonic antigen (CEA) standard solution (1.0 mg mL^{-1}) was supplied by Shanghai Linc-Bio Science Company, Ltd. (Shanghai, China). Mouse monoclonal capture antibody (primary antibody, Ab_1, clone no. 27D6), polyclonal signal antibody (secondary antibody, Ab_2, clone no. 28E4) and HRP-labeled Ab_2 were purchased from the Shuangliu Zhenglong Biochemistry Lab (Chengdu, China). 0.1 M phosphate buffer salines (PBS) with various pHs were prepared by mixing the stock solutions of 0.1 M NaH_2PO_4 and 0.1 M Na_2HPO_4 containing 0.1 M KNO_3 as the supporting electrolyte. The washing buffer was 0.05% (w/v) Tween-20 (PBST) in 0.01 M pH 7.4 PBS. The blocking solution was 0.01 M pH 7.4 PBS containing 5% (w/v) BSA. The clinical serum samples were fetched from Jiangsu Institute of Cancer Prevention and Cure. All the other reagents were of analytical grade and used as received. Ultrapure water obtained from a Millipore water purification system (≥18 MΩ, Milli-Q, Millipore) was used in all assays.

Apparatus. UV−vis absorption spectra were recorded on a UV-3600 UV−Vis−NIR spectrophotometer (Shimadzu Company, Japan). Attenuated total reflection Fourier transformation infrared (ATR-FTIR) spectra were obtained with a Vector 22 FTIR spectrometer (Bruker Optics, Germany). X-ray photoelectron spectral (XPS) experiments were operated on an ESCALAB 250 spectrometer (Thermo-VG Scientific Company). The transmission electron micrograph (TEM) was obtained using a JEM-2100 TEM instrument (JEOL). The morphologies of sample films were examined under an S-4800 field-emission scanning electron microscope (FESEM) (Hitachi) after they were coated with Au films to improve the conductivity. Tapping mode atomic force microscopic (AFM) images were acquired under ambient conditions using an Agilent 5500 AFM/SPM system with Picoscan, v5.3.3. The samples were prepared via directly casting thin aqueous dispersions (~0.1 mg mL^{-1}) of NG and hemin@NG onto freshly cleaved mica sheets. After being dried overnight at room temperature, the samples were rinsed with drips of water to wash away loosely immobilized samples and dried prior to measurement. The static water contact angles were measured at 20 °C by a Dataphysics OCA-30 contact angle meter, employing deionized water drops. The ζ potential was measured by a Nano-Z Zetasizer nanoparticle analyzer (Malvern Instruments Ltd.). Electrochemical experiments were performed on a CHI 812B electrochemical workstation (CH Instruments Inc.), and electrochemiluminescent (ECL) measurements were carried out in a self-made cell on a MPI-E multifunctional electrochemical and chemiluminescent analytical system (Xi'an Remex Analytical Instrument Company, Ltd. China) with a conventional three-electrode configuration consisting of a modified glassy carbon electrode (GCE, 5 mm in diameter) as the working electrode, a platinum wire as the counter electrode, and a Ag/AgCl (saturated KCl as filling liquid) as the reference electrode. All potentials were quoted against this reference. The ECL emission window was placed above the photomultiplier tube (PMT, detection range: 300−650 nm) biased at −1000 V. Unless specifically mentioned, the scan rate was 100 mV s^{-1}. The reference levels of CEA in human serum samples were detected with an automated electrochemiluminescent analyzer (Elecsys 2010, Roche).

Preparation of NG. Aluminophosphate nanoroll as a precursor of NG was prepared using mixed organoamines via a biomimetic synthesis.[24] The precursor was heated at 700 °C for 14 h under argon. After cooling down, the black powder and 37% hydrochloric acid were sealed into a Teflon-lined autoclave for heating in an oven at 160 °C for 18 h. To obtain the pristine NG, the resulting black solid product was collected by centrifugation, washed by water, and anhydrous ethanol repeatedly, and dried under vacuum at 60 °C for 12 h.

Preparation of Hemin@NG. A certain amount of NG was first treated by ultrasonicating in a mixture of concentrated sulfuric acid:nitric acid (3:1, v/v) at 60 °C for 4 h. The

dx.doi.org/10.1021/ac3036537 | Anal. Chem. 2013, 85, 5390−5396

suspension was centrifuged and washed with ultrapure water until the filtrate pH approximated 7. After being dried at 50 °C overnight, the carboxylated NG was exfoliated by ultrasonicating a 0.1 wt % dimethylformamide (DMF) dispersion for 30 min at the frequency of 53 kHz. Unexfoliated graphene nanosheets were removed by a 5 min centrifugation at 2000 rcf. Then, 1.0 mL hemin in DMF at 1 mM was introduced into 6.0 mL DMF dispersion of 0.1 mg mL^{-1} NG and shaken by a vortex mixer at room temperature for 10 h. After centrifugation at 14000 rcf for 30 min, the obtained precipitate was thrice washed with DMF and ultrapure water to obtain hemin@NG and then redispersed in 1.0 mL ultrapure water. Similarly, hemin@GO was prepared as the control.

Preparation of Hemin@NG-Labeled Ab_2. Five-hundred microliters of the above solution was mixed with 500 μL of 400 mM EDC and 100 mM NHS in 0.1 M pH 6.0 MES buffer and vibrated softly at room temperature for 20 min. After the resulting mixture was centrifuged at 14000 rcf for 10 min, and then washed twice with 10 mM pH 7.4 PBS to remove excessive EDC and NHS, the precipitate was redispersed in 1 mL ultrapure water. Twenty microliters of 50 μg mL^{-1} Ab_2 was then added to the dispersion, which was vortexed mildly at room temperature for 4 h, centrifuged at 6000 rcf for 10 min, and twice washed with 10 mM pH 6.0 PBS to obtain the hemin@NG-labeled Ab_2 bioconjugate. Finally, the bioconjugate was redispersed in 10 mM pH 7.4 PBS containing 0.5% BSA and stored at 4 °C for further application. Hemin@GO-labeled Ab_2 bioconjugate was also prepared in a similar way.

Construction of ECL Immunosensor. The DMSA-stabilized CdTe QDs were prepared according to the reported electrolysis method.[25] After the electrolysis step, the resulting solution was airproofed at 80 °C for 20 h to harvest QDs. The as-prepared QDs solution was sedimentated in 1:1 (v/v) isopropyl alcohol/water and centrifuged at 6000 rcf for 10 min. In accordance with Peng's empirical equation,[26] the concentration of redispersed QDs solution was estimated to be ~10 μM with a size of 1.2 nm. Twenty microliters of the QDs solution was then cast onto a pretreated GCE surface to act as the ECL nanoemitters. Prior to the modification, the electrode was polished to a mirrorlike finish, using 0.3 and 0.05 μm alumina slurry (Beuhler) followed by sonication in absolute ethanol and ultrapure water, rinsing thoroughly with ultrapure water and drying under a N_2 flow.

Ten microliters of chitosan solution (0.025 wt %) was coated on the QD film-modified GCE for covalent binding with the *anti*-CEA antibody by activating the chitosan film with 15 μL of 2% glutaraldehyde in 0.01 M pH 7.4 PBS for 2 h and then incubating it in 20 μL of Ab_1 (50 μg mL^{-1}) for 60 min at 36 and 4 °C overnight in a 100% moisture-saturated environment. The resulting surface was slowly washed with streams of PBST and PBS to remove the physically absorbed Ab_1, and then blocked with 20 μL of 5% BSA solution for 1 h at 36 °C, and finally washed with PBST and PBS again to form the ECL immunosensor.

Measurement Procedure. A sandwich-type immunoassay was performed for the antigen detection. The immunosensor was first incubated with 20 μL of CEA standard solution or serum sample at 36 °C for 30 min. After a washing step, 20 μL of hemin@NG-labeled Ab_2 was pipetted on the immunosensor for 60 min incubation at 36 °C, followed by washing again. Finally, the ECL signal was detected in air-saturated 0.1 M pH 8.0 PBS.

RESULTS AND DISCUSSION

Characterization of Hemin@NG. Carboxylic NG was chosen as the nanocarrier for preparation of the hemin-based

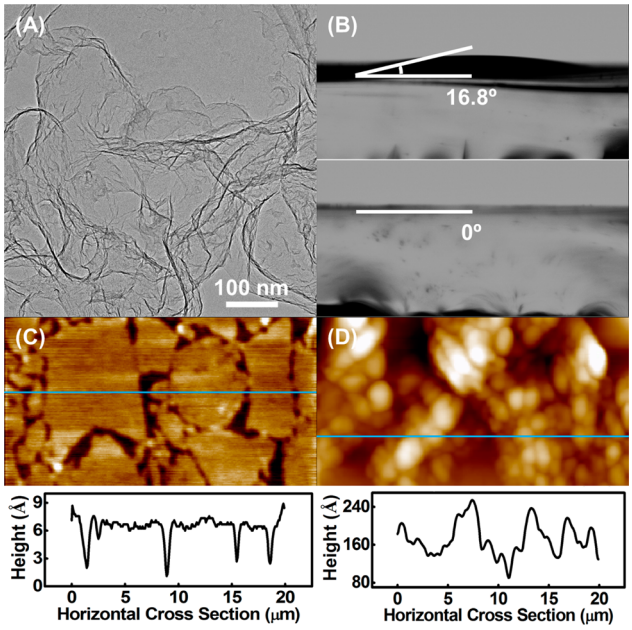

Figure 1. (A) TEM image of pristine NG. (B) Photographic illustration of contact angles of NG (upper) and hemin@NG (lower)-modified ITO slides. AFM topographic images of (C) carboxylated NG and (D) hemin@NG with corresponding height profile of the horizontal cross section.

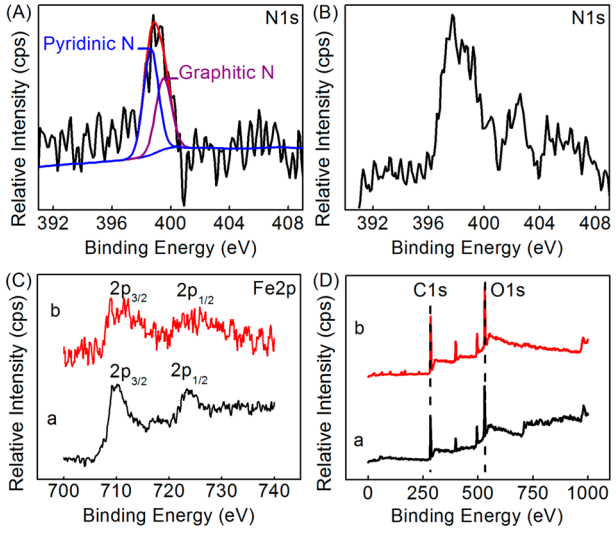

Figure 2. XPS N1s spectra of (A) NG and (B) hemin@NG. (C) XPS Fe2p spectra and (D) XPS survey scan of (a) hemin and (b) hemin@NG.

electrocatalyst. The bright-field TEM image revealed that the NG film consisted of randomly thin, aggregated, and crumpled sheets with large specific areas (Figure 1A), which benefited the high loading of hemin for enhancing the catalytic efficiency of the probe. The acidization and oxidation of NG was considered to produce carboxylic groups mainly around the edge planes[27] and resulted in an overall spreading topography due to the

dx.doi.org/10.1021/ac3036537 | *Anal. Chem.* 2013, 85, 5390−5396

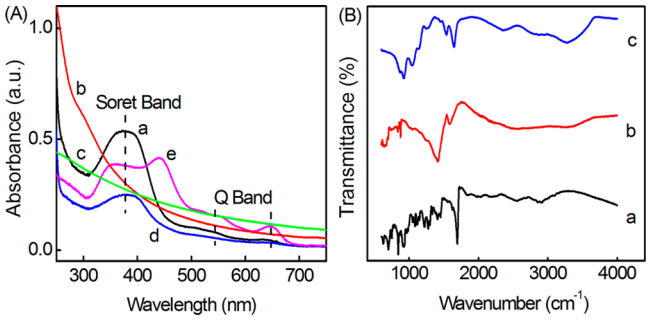

Figure 3. (A) UV−vis of (a) hemin, (b) GO, (c) NG, (d) hemin@GO, and (e) hemin@NG. (B) ATR-FTIR spectra of (a) hemin, (b) hemin@NG, and (c) hemin@NG-labeled Ab_2.

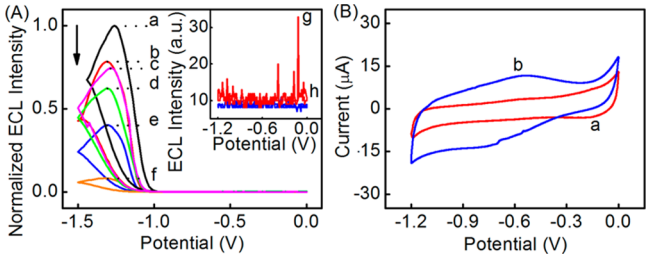

Figure 4. (A) ECL responses of the immunosensor in air-saturated 0.1 M pH 8.0 PBS (a) before and after incubation with 10 ng mL^{-1} CEA and then (b) Ab_2, (c) NG-labeled Ab_2, (d) HRP-labeled Ab_2, (e) hemin@GO-labeled Ab_2, and (f) hemin@NG-labeled Ab_2. Inset: ECL behaviors of (g) GO- and (h) NG-modified GCEs. (B) CVs of (a) GO- and (b) NG-modified GCEs in air-saturated 0.1 M pH 8.0 PBS.

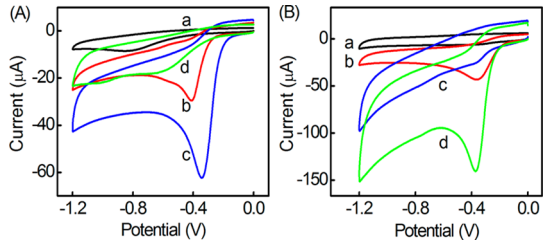

Figure 5. (A) CVs of the immunosensor in air-saturated 0.1 M pH 8.0 PBS after incubation with 10 ng mL^{-1} CEA and then (a) HRP-, (b) hemin@GO-, (c) hemin@NG-, and (d) NG-labeled Ab_2. (B) CVs of (a and b) hemin- and (c and d) hemin@NG-modified GCEs in (a and c) N_2- and (b and d) air-saturated 0.1 M pH 8.0 PBS.

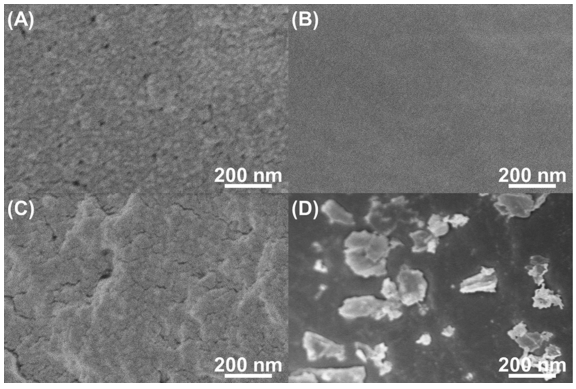

Figure 6. FESEM images of (A) DMSA-CdTe QDs, (B) QDs/chitosan, (C) QDs/chitosan/Ab_1/CEA, and (D) QDs/chitosan/Ab_1/CEA/hemin@NG-labeled Ab_2 modified GCE.

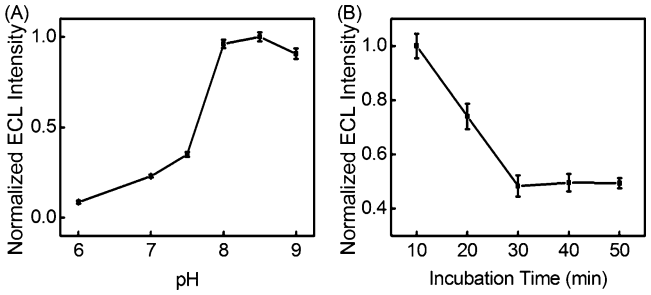

Figure 7. Effects of (A) pH value of detection solution and (B) incubation time for CEA on ECL intensity of hemin@NG-Ab_2-bound immunosensor in air-saturated 0.1 M PBS.

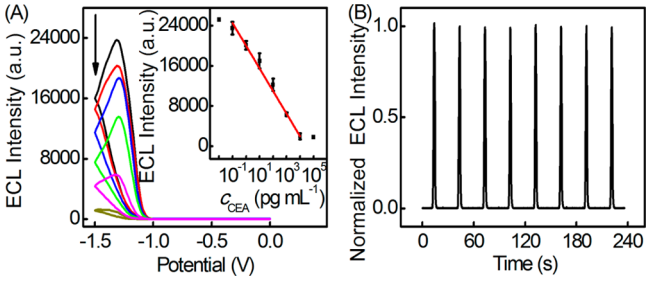

Figure 8. (A) ECL responses of the QD-based immunosensor to CEA at 0.1, 1.0, 10, and 100 pg mL^{-1} and 1.0 and 10 ng mL^{-1} (from top to bottom) in air-saturated 0.1 M pH 8.0 PBS. Inset: calibration curve. (B) Continuous cyclic scans of the immunosensor in air-saturated 0.1 M pH 8.0 PBS after incubation with 10 ng mL^{-1} of CEA and then hemin@NG-labeled Ab_2.

electrostatic repulsion among each individual graphene nanosheet.[28]

The hydrophilicity of an interface can be qualitatively characterized by measuring the contact angle of the substrate. The contact angle of the NG film modified ITO slide was measured to be 16.8° (Figure 1B), indicating good hydrophilicity, which could be ascribed to the multiple defects from nitrogen doping and more hydrophilic groups produced by acidic treatment.[27] The instantaneous near-zero angle of hemin@NG film upon contact of the water droplet indicated much better hydrophilicity and much lower surface tension of the hemin@NG than that of NG itself, as the supported hemins introduced a great deal of carboxylic groups on the NG surface. These carboxylic groups also led to the change of the ζ potential data from −29.6 mV of NG to −41.1 mV of hemin@NG, which greatly improved the aqueous dispersity of NG.[29]

Tapping mode AFM gave the horizontal cross-sectional profile of carboxylic NG, which showed an average thickness of ~0.5 nm (Figure 1C), corresponding to an atomic monolayer nature.[30] After assembling hemin on NG, the thickness increased to ~6.0 nm (Figure 1D). The NG was slightly thinner than chemical converted GO (e.g., ~1.0 nm) with multiple O-functionalities grafted on its basal plane.[30]

Interaction Between Hemin and NG. The XPS was first applied to characterize the interaction between hemin and NG. The N1s XPS of NG exhibited two well-separated peaks, attributed to the pyridinic and graphitic N at 399.6 and 398.7 eV (Figure 2A), respectively, with an N/C atomic abundance ratio of 5.24% calculated from the XPS survey scan. After the assembly of hemin, the N1s XPS peak of hemin@NG occurred at 397.6 eV (Figure 2B). The coordination could be verified by comparing the $Fe2p_{3/2}$ peak of Fe−N in hemin and hemin@

dx.doi.org/10.1021/ac3036537 | Anal. Chem. 2013, 85, 5390−5396

Table 1. Assay Results of Clinical Serum Samples Using the Proposed and Reference Methods

sample no.	1[a]	1[b]	1[c]	1[d]	1[e]	2[b]	2[e]	3[b]	3[e]
proposed method (pg mL^{-1})	0.380	3.92	37.8	386	3881	2.45	2775	2.28	2257
reference method (pg mL^{-1})	0.355	3.55	35.5	355	3550	2.62	2620	2.09	2090
relative error (%)	7.0	10.4	6.5	8.7	9.3	−6.5	5.9	9.1	8.0

[a]The serum samples were diluted 1 × 10^4 times. [b]The serum samples were diluted 1000 times. [c]The serum samples were diluted 100 times. [d]The serum samples were diluted 10 times. [e]The serum samples were not diluted.

NG. The former occurred at 710.2 eV (Figure 2C, curve a), and the latter shifted to a higher energy at 711.4 eV (Figure 2C, curve b). This shift should be attributed to the presence of electron-donating pyridinic N atoms of NG that coordinated the central Fe atom of hemin. Upon the coordination assembly of hemin, the ratio of integral peak areas of pyridinic to graphitic N decreased, which suggested some part of pyridinic N converted into ferric N after the formation of hemin@NG, and the N/C atomic abundance ratio increased to 6.18%, indicating a growing relative concentration of N in pyrrolic groups of hemin. Furthermore, in accordance with the XPS survey scan (Figure 2D), the relative atomic abundance ratio of C1s/Fe2p in hemin (Figure 2D, curve a) and hemin@NG (Figure 2D, curve b) were measured to be 35.4 and 54.5, respectively. The higher content of the C atom in hemin@NG was attributed to the carbon backbone of graphene. Considering that the positively charged ferric ion was electrophilic to the N atom with relatively high local electronegativity in NG,[31] the hemin@NG might be formed through site-specific Fe−N axial coordination. Meanwhile, owing to the π-electron delocalization of graphene and the porphyrin ring of hemin, the noncovalent π-stacking interaction should have also occurred in the attachment of hemin onto NG. The ligation should be between the Fe atom and pyridinic N dopant in the backbone of graphene.[32] The thickness of ∼6.0 nm for hemin@NG verified that the axial ligation of hemin on NG was in a sandwich type.[32]

The interaction of hemin with NG was further characterized by UV−vis spectra (Figure 3A). Hemin featured an intense Soret band at 373 nm together with weak Q bands at longer wavelengths of 531 and 646 nm (Figure 3A, curve a).[17] The absorptive hyperchromicity in visible and near-infrared ranges (Figure 3A, curves b and c) and the color change from yellow brown to gray black due to the doping of the N atom suggested higher conjugation of the NG nanosheet than the GO.[33] After hemin was mixed with NG, the Soret band of formed hemin@NG was split into two adsorption peaks at 356 and 439 nm, and the Q bands occurred at the same wavelengths (Figure 3A, curve e). Contrarily, the assembly of hemin on GO only led to a slight red shift of the Soret band for around 17 nm (Figure 3A, curve d), due to the molecular flattening.[34] The peak at 356 nm could be attributed to the assembly of hemin on NG by Fe−N coordination,[19] while the peak at 439 nm resulted from the $\pi-\pi$ noncovalent interaction between NG and the porphine ring of the hemin axially assembled on NG.[35] Due to the 1:1 stoichiometric ratio of the Fe atom to protoporphyrin ring, the two Soret bands showed near peak intensities. The coexistence of two kinds of interactions strengthened the association between NG and hemin, which was desirable to prevent the leakage of hemin from hemin@NG. In accordance with the Beer−Lambert law, the loading capacity of hemin on the surface of NG and GO was estimated to be 2.45 and 1.44 μmol g^{-1}, respectively, which implied that NG was a more efficient nanocarrier than GO.

Characterization of Hemin@NG-Ab$_2$. The FTIR spectrum in the fingerprint region of hemin showed the side-chain carboxy ethyl, vinyl, and methyl groups of the protoporphyrin ring (Figure 3B, curve a).[36] The sharp band at 1706 cm^{-1} corresponded to the C═O stretch of the carboxylic acid groups.[37] In comparison with the FTIR spectra of hemin and hemin@NG (Figure 3B, curve b), the FTIR spectrum of hemin@NG-labeled Ab$_2$ displayed obvious vibration peaks corresponding to the featured amide bands of proteins [e.g., amide I (1650 cm^{-1}) for C═O stretching and amide II (1539 cm^{-1}) for N−H bending/C−N stretching, respectively (Figure 3B, curve c)],[38] which confirmed that the antibody was successfully linked with hemin@NG by the amidation reaction.

ECL Quenching Mechanism by Hemin@NG. The chitosan/QDs/GCE showed an efficient cathodic ECL emission in air-saturated pH 8.0 PBS with an emission peak at −1.26 V (Figure 4A, curve a). In the ECL emission process, dissolved oxygen was demonstrated to produce an endogenous coreactant H_2O_2 by its electrochemical reduction on the electrode surface.[8] After the chitosan was bound with capture antibody to perform the sandwich-type immunoreactions with 10 ng mL^{-1} antigen and Ab$_2$, the steric hindrance led to a decrease of the ECL emission by 22.6% (Figure 4A, curve b). However, when the Ab$_2$ was replaced with NG-, HRP-, hemin@GO-, and hemin@NG-labeled Ab$_2$, the ECL intensity decreased by 25.4%, 37.8%, 59.8%, and 91.8%, respectively (Figure 4A, curves c, d, e, and f). Obviously, the presence of HRP further increased the steric hindrance for ECL emission. However, the steric hindrance from NG-, hemin@GO-, and hemin@NG-labeled Ab$_2$ could not lead to such change because carbon nanomaterials could promote the charge transfer for sensitizing the ECL emission.[39] Moreover, neither the GO nor the NG nanosheet itself could produce ECL irradiation (inset in Figure 4A, curves g and h). Thus, the decrease of ECL emission resulted from the other quenching mechanism.

To clarify the mechanism, the CVs of immunosensors after incubation with CEA and then HRP-, hemin@GO-, and hemin@NG-labeled Ab$_2$ were examined in the potential window of the oxygen reduction (Figure 5A). The immunosensor incubated with HRP-labeled Ab$_2$ showed a reduction peak at −0.79 V (Figure 5A, curve a), which resulted from the electrochemical reduction of dissolved oxygen to generate a small amount of H_2O_2. The reduction peak shifted to −0.63 V in the presence of NG-labeled Ab$_2$ (Figure 5A, curve d). The potential shift resulted from the promotion of NG to the electrochemical reduction, which led to greater peak current. After the immunosensor was incubated with hemin@GO- and hemin@NG-labeled Ab$_2$, respectively, the reduction peak at −0.79 V disappeared and a well-defined new peak occurred at −0.41 and −0.35 V, respectively (Figure 5A, curves b and c), which could be attributed to the electrocatalytic activity of hemin@GO and hemin@NG toward the reduction of dissolved oxygen to H_2O or OH^-. Both the more positive reduction potential and twice larger reduction current in the

dx.doi.org/10.1021/ac3036537 | Anal. Chem. 2013, 85, 5390−5396

presence of hemin@NG suggested the more efficient catalytic activity and higher loading capacity of hemin on NG than GO, which was ascribed to the different assembly mechanisms of two mimetic enzymes. Furthermore, compared with the electrocatalytic performance toward oxygen reduction at NG-labeled Ab_2 (Figure 5A, curve d), hemin@NG-labeled Ab_2 (Figure 5A, curve c) showed a much larger peak current along with more positive peak potential. Therefore, the presence of the N atom as the active sites in NG could act as an electron donor to promote the reactivity of adsorbed hemin and facilitate the electrocatalytic reduction of O_2.[21,22] Thus hemin@NG showed greater quenching efficiency on the cathodic ECL emission of QDs (Figure 4A, curves c and f).

At hemin-modified GCE, a tiny peak could be observed at about −0.30 V in N_2-saturated atmosphere (Figure 5B, curve a), which was attributed to the direct electrochemistry of hemin. In the presence of dissolved oxygen, the reduced form of hemin could quickly be oxidized by dissolved oxygen to transform O_2 into OH^- in the basic condition, leading to an enhanced reduction peak (Figure 5B, curve b). Relatively, the oxygen reduction currents at both GO- and NG-modified GCEs were negligible (Figure 4B). As expected, hemin@NG modified GCE showed a much greater reduction peak of hemin with a slightly positive shift than hemin-modified GCE (Figure 5B, curve c), indicating the accelerated electron transfer and the high loading of hemin, thus the modified electrode showed a greater reduction peak current of O_2 in an air-saturated environment (Figure 5B, curve d). The electrochemical process could be described by the following equations:

$$\text{Hemin[Fe(III)]@NG} + e^- \rightarrow \text{Hemin[Fe(II)]@NG} \quad (1)$$

$$4\text{Hemin[Fe(II)]@NG} + O_2 + 2H_2O \rightarrow 4\text{Hemin[Fe(III)]@NG} + 4OH^- \quad (2)$$

Equation 2 led to the consumption of dissolved oxygen, which greatly prevented the formation of H_2O_2 as the ECL coreactant to quench ECL emission. Therefore, the hemin@NG could be used as a highly efficient signal tag for the ECL immunoassay. After the immunorecognition between hemin@NG-labeled Ab_2 and antigen, the FESEM images showed individual NG nanosheets on the immunosensing interface without aggregation of graphene sheets (Figure 6), which might improve the quenching efficiency of the biosensing platform.

Condition Optimization and Performance of Immunoassay. To apply hemin@NG-labeled Ab_2 in the ECL immunoassay, several experimental parameters, including the pH of the detection solution and the incubation time of antigen, should be optimized. The effect of pH on the ECL response of QDs was shown in Figure 7A. In the examined pH range, the ECL intensity increased with the increasing pH value and then reached a plateau at pH 8.0. This result could be attributed to the fact that the electrogenerated intermediates (e.g., $O_2^{\bullet-}$ and $HO^{\bullet}$) of dissolved O_2 and the resulting H_2O_2 were more stable at high pH, which was favorable for the improvement of the ECL emission. Although the maximal QD-based ECL response emerged at pH 8.5, considering the bioactivity of immunoreagents and the approximating ECL intensity at both pH values, pH 8.0 PBS was selected as the detection solution.

At room temperature, the ECL quenching increased and tended to a constant state after 30 min with the increasing incubation time employed in a sandwich-type immunoassay (Figure 7B), which showed a saturated binding of the analyte to the capture antibody on the immunosensor surface. Therefore, 30 min of incubation time was selected for the sandwich-type immunoassay.

Under the optimum conditions, the ECL intensity of the immunosensor decreased with the increasing concentration of CEA in the incubation solution (Figure 8A). The calibration plot showed a good linear relationship between the ECL intensity and the logarithmic value of CEA concentration in the range from 0.1 pg mL^{-1} to 10 ng mL^{-1}, with a correlation coefficient of 0.992 (inset in Figure 8A). The detection limit at a signal-to-noise ratio of 3 was 24 fg mL^{-1}, which was about 20 times lower than those previously reported by the electrochemical and ECL immunoassay with different amplification strategies.[40,41] Since the concentration range of CEA in the normal serum is 0−5 ng mL^{-1},[42] the analytical performance of the proposed method indicated its good practicality in clinic diagnoses. More importantly, this immunoassay method showed a wide detection range of 5 orders of magnitude and avoided the need for deoxygenating with the electrochemical immunoassay.

Reproducibility, Precision, and Application. The intra-assay and interassay precisions of the ECL immunosensor were examined by detecting 0.1 ng mL^{-1} CEA. The relative standard deviation (RSD) for twenty measurements of CEA with the same immunosensor was 4.9%, while the RSD for twenty parallel measurements with twenty immunosensors was 8.5%, indicating good precision of the immunoassay method and acceptable fabrication reproducibility of the immunosensors. Eight measurements of ECL emission from the immunosensor at 0.1 ng mL^{-1} CEA upon continuous cyclic scans showed a coincident signal with RSD of 1.7% (Figure 8B), indicating acceptable reliability and stability of the detection signal.

The analytical reliability and application potential of the proposed method were evaluated by comparing the assay results of clinical serum samples with the reference values obtained by commercial electrochemiluminescent single-analyte tests (Table 1). When the level of CEA was over the calibration range, the serum sample was appropriately diluted with 0.1 M pH 8.0 PBS, prior to assaying. The results indicated acceptable accuracy of the proposed method for the detection of CEA even in undiluted serum samples. In consideration of the CEA threshold of 0.1 ng mL^{-1} for clinic diagnoses, the proposed method possessed good practicability.

■ CONCLUSIONS

This work demonstrated a facile pathway to fabricate a universal biomimetic electrocatalyst by sandwich-typed assembly of hemin on NG via the axial ligation and π-stacking interaction, which is favorable to restore the primitive enzyme environment. The $\pi-\pi$ interaction between NG and protoporphyrin ring of the axially assembled hemin further strengthens their association. The novel assembly mechanism endows hemin@NG with much higher loading capacity and more efficient catalytic activity than other hemin-based mimetic enzymes, such as hemin@GO. The hemin@NG shows highly efficient electrocatalytic activity toward the reduction of O_2 via a four-electron pathway, which greatly prevents the formation of H_2O_2 as a QD-based ECL coreactant, and thus quenches the ECL emission of QDs. Following this coreactant consumption mechanism, a novel immunoassay methodology for ultrasensitive ECL detection of protein has been developed by using the hemin@NG as a signal tag. This method shows a wide

dx.doi.org/10.1021/ac3036537 | Anal. Chem. 2013, 85, 5390−5396

linear range over 5 orders of magnitude and a detection limit of subpicogram per milliliter. The good performance of the proposed method indicates the potential application of the hemin@NG in the bioassay. The assembly mechanism of the mimetic enzyme could easily be extended to other porphyrin derivatives.

AUTHOR INFORMATION

Corresponding Author

*E-mail: hxju@nju.edu.cn. Tel/Fax: +86-25-83593593.

Notes

The authors declare no competing financial interest.

ACKNOWLEDGMENTS

This work was financially supported by the National Basic Research Program of China (Grant 2010CB732400), National Natural Science Foundation of China (Grants 21121091 and 21135002), and Excellent Talents in Chinese Universities (Grant NCET100479).

REFERENCES

(1) Ferrari, M. *Nat. Rev. Cancer* **2005**, *5*, 161−171.
(2) Munge, B. S.; Coffey, A. L.; Doucette, J. M.; Somba, B. K.; Malhotra, R.; Patel, V.; Gutkind, J. S.; Rusling, J. F. *Angew. Chem., Int. Ed.* **2011**, *50*, 7915−7918.
(3) Chai, J. A.; Wong, L. S.; Giam, L.; Mirkin, C. A. *Proc. Natl. Acad. Sci. U.S.A.* **2011**, *108*, 19521−19525.
(4) Ju, H. X. *Sci. China: Chem.* **2011**, *54*, 1202−1217.
(5) Chou, S. S.; De, M.; Luo, J. Y.; Rotello, V. M.; Huang, J. X.; Dravid, V. P. *J. Am. Chem. Soc.* **2012**, *134*, 16725−16733.
(6) Wang, J.; Han, H. Y.; Jiang, X. C.; Huang, L.; Chen, L. N.; Li, N. *Anal. Chem.* **2012**, *84*, 4893−4899.
(7) Lei, J. P.; Ju, H. X. *Chem. Soc. Rev.* **2012**, *41*, 2122−2134.
(8) Liu, X.; Zhang, Y. Y.; Lei, J. P.; Xue, Y. D.; Cheng, L. X.; Ju, H. X. *Anal. Chem.* **2010**, *82*, 7351−7356.
(9) Song, Y. J.; Qu, K. G.; Zhao, C.; Ren, J. S.; Qu, X. G. *Adv. Mater.* **2010**, *22*, 2206−2210.
(10) Du, D.; Wang, L. M.; Shao, Y. Y.; Wang, J.; Engelhard, M. H.; Lin, Y. H. *Anal. Chem.* **2011**, *83*, 746−752.
(11) Yu, X.; Munge, B.; Patel, V.; Jensen, G.; Bhirde, A.; Gong, J. D.; Kim, S. N.; Gillespie, J.; Gutkind, J. S.; Papadimitrakopoulos, F.; Rusling, J. F. *J. Am. Chem. Soc.* **2006**, *128*, 11199−11205.
(12) Cunnington, A. J.; de Souza, J. B.; Walther, M.; Riley, E. M. *Nat. Med.* **2012**, *18*, 120−127.
(13) Fry, H. C.; Garcia, J. M.; Medina, M. J.; Ricoy, U. M.; Gosztola, D. J.; Nikiforov, M. P.; Palmer, L. C.; Stupp, S. I. *J. Am. Chem. Soc.* **2012**, *134*, 14646−14649.
(14) Bruice, T. C. *Acc. Chem. Res.* **1991**, *24*, 243−249.
(15) Pelossof, G.; Tel-Vered, R.; Elbaz, J.; Willner, I. *Anal. Chem.* **2010**, *82*, 4396−4402.
(16) Freeman, R.; Liu, X. Q.; Willner, I. *J. Am. Chem. Soc.* **2011**, *133*, 11597−11604.
(17) Xue, T.; Jiang, S.; Qu, Y. Q.; Su, Q.; Cheng, R.; Dubin, S.; Chiu, C. Y.; Kaner, R.; Huang, Y.; Duan, X. F. *Angew. Chem., Int. Ed.* **2012**, *124*, 3888−3891.
(18) Zhang, G. F.; Dasgupta, P. K. *Anal. Chem.* **1992**, *64*, 517−522.
(19) Lefèvre, M.; Dodelet, J. P.; Bertrand, P. *J. Phys. Chem. B* **2002**, *106*, 8705−8713.
(20) Tu, W. W.; Lei, J. P.; Jian, G. Q.; Hu, Z.; Ju, H. X. *Chem.—Eur. J.* **2010**, *16*, 4120−4126.
(21) Gong, K. P.; Du, F.; Xia, Z. H.; Durstock, M.; Da, L. M. *Science* **2009**, *323*, 760−764.
(22) Tang, Y. F.; Allen, B. L.; Kauffman, D. R.; Star, A. *J. Am. Chem. Soc.* **2009**, *131*, 13200−13201.
(23) Wang, X. F.; Zhou, Y.; Xu, J. J.; Chen, H. Y. *Adv. Funct. Mater.* **2009**, *19*, 1−7.
(24) Guo, X. K.; Ma, Q. L.; Guo, X. F.; Ding, W. P.; Chen, Y. *Chem. Commun. (Cambridge, U.K.)* **2009**, *45*, 3443−3445.
(25) Ge, C. W.; Xu, M.; Liu, J.; Lei, J. P.; Ju, H. X. *Chem. Commun. (Cambridge, U.K.)* **2008**, *4*, 450−452.
(26) Yu, W. W.; Qu, L. H.; Guo, W. Z.; Peng, X. G. *Chem. Mater.* **2003**, *15*, 2854−2860.
(27) Burch, H. J.; Brown, E.; Contera, S. A.; Toledo, N. C.; Cox, D. C.; Grobert, N.; Hao, L.; Ryan, J. F.; Davies, J. A. *J. Phys. Chem. C* **2008**, *112*, 1908−1912.
(28) Li, D.; Muller, M. B.; Gilje, S.; Kaner, R. B.; Wallace, G. G. *Nat. Nanotechnol.* **2008**, *3*, 101−105.
(29) Wu, L.; Wang, J. S.; Feng, L. Y.; Ren, J. S.; Wei, W. L.; Qu, X. G. *Adv. Mater.* **2012**, *24*, 2447−2452.
(30) Stankovich, S.; Dikin, D. A.; Dommett, G. H. B.; Kohlhaas, K. M.; Zimney, E. J.; Stach, E. A.; Piner, R. D.; Nguyen, S. T.; Ruoff, R. S. *Nature* **2006**, *442*, 282−286.
(31) Lepró, X.; Vega-Cantú, Y.; Rodríguez-Macías, F. J.; Bando, Y.; Golberg, D.; Terrones, M. *Nano Lett.* **2007**, *7*, 2220−2226.
(32) Offord, D. A.; Sachs, S. B.; Ennis, M. S.; Eberspacher, T. A.; Griffin, J. H.; Chidsey, C. E. D.; Collman, J. P. *J. Am. Chem. Soc.* **1998**, *120*, 4478−4487.
(33) Sun, X. M.; Liu, Z.; Welsher, K.; Robinson, J. T.; Goodwin, A.; Zaric, S.; Dai, H. J. *Nano Res.* **2008**, *1*, 203−212.
(34) Xu, Y. X.; Zhao, L.; Bai, H.; Hong, W. J.; Li, C.; Shi, G. Q. *J. Am. Chem. Soc.* **2009**, *131*, 13490−13497.
(35) Chen, J. Y.; Collier, C. P. *J. Phys. Chem. B* **2005**, *109*, 7605−7609.
(36) Paneque, A.; Fernández-Bertrán, J.; Reguera, E.; Yee-Madeira, H. *Struct. Chem.* **2003**, *14*, 551−558.
(37) Tom, R. T.; Pradeep, T. *Langmuir* **2005**, *21*, 11896−11902.
(38) Zhang, J.; Lei, J. P.; Xu, C. L.; Ding, L.; Ju, H. X. *Anal. Chem.* **2010**, *82*, 1117−1122.
(39) Li, L. L.; Liu, K. P.; Yang, G. H.; Wang, C. M.; Zhang, J. R.; Zhu, J. J. *Adv. Funct. Mater.* **2011**, *21*, 869−878.
(40) Mani, V.; Chikkaveeraiah, B. V.; Patel, V.; Gutkind, J. S.; Rusling, J. F. *ACS Nano* **2009**, *3*, 585−594.
(41) Deng, S. Y.; Lei, J. P.; Huang, Y.; Yao, X. N.; Ding, L.; Ju, H. X. *Chem. Commun. (Cambridge, U.K.)* **2012**, *48*, 9159−9161.
(42) Ishigami, S.; Natsugoe, S.; Hokita, S.; Che, X. M.; Tokuda, K.; Nakajo, A.; Iwashige, H. *J. Clin. Gastroenterol.* **2001**, *1*, 41−44.